Wear 270 (2011) 828–838

Contents lists available at ScienceDirect

Wear

journal homepage: www.elsevier.com/locate/wear

In situ monitoring and prediction of progressive joint wear using Bayesian statistics

Dawn An [a], Joo-Ho Choi [a], Tony L. Schmitz [b], Nam H. Kim [b,*]

[a] Korea Aerospace University, Aerospace & Mechanical Engineering, 100 Hanggongdae-gil, Hwajeon-dong, Deokyang-gu, Goyang-City, Gyeonggi-do, 412-791, South Korea
[b] University of Florida, Mechanical & Aerospace Engineering, 210 MAEA, P.O. Box 116250, Gainesville, FL 32611-6250, USA

ARTICLE INFO

Article history:
Received 12 August 2010
Received in revised form 10 February 2011
Accepted 16 February 2011
Available online 23 February 2011

Keywords:
Wear
Capacitance probe
Prognosis
Uncertainty
Bayesian inference
Slider–crank mechanism

ABSTRACT

In this paper, a statistical methodology of estimating wear coefficient and predicting wear volume in a revolute joint using in situ measurement data is presented. An instrumented slider–crank mechanism that can measure the joint force and the relative motion between the pin and bushing is built. The former is measured using a load cell built onto a necked portion of the hollow steel pin, while the latter is measured using a capacitance probe. In order to isolate the effect of friction in other joints, a porous carbon air bearing for the revolute joint between the follower link and the slide stage, as well as a prismatic joint for the linear slide, are used. Based on the relative motion between the centers of the pin and bushing, the wear volumes are estimated at six different operating cycles. The Bayesian inference technique is used to update the distribution of wear coefficients, which incorporates in situ measurement data to obtain the posterior distribution. The Markov Chain Monte Carlo technique is employed to generate samples from the given distribution. The results show that it is possible to narrow the distribution of wear coefficients and to predict the future wear volume with reasonable confidence. The effect of the prior distribution on the wear coefficient is discussed by comparing with the non-informative case.

1. Introduction

Mechanical systems are characterized by motion. In order to fulfill their design function, the individual components of a system must move relative to one another, which inevitably produces sliding along the mating surfaces and causes wear. Wear is the gradual removal of material from contacting surfaces in relative motion, which eventually causes failure of the system. Since mechanical wear occurs for most systems in motion, it is important to predict its effects and estimate the service life of the system before failure.

The traditional practice of predicting service life of a mechanical component under wear is performed through three stages [1–3]. First, the material wear coefficient is measured using a tribometer to approximate the actual conditions. Normally, a constant load is applied on the two mating surfaces under rotational or reciprocating motion. Second, the contact pressure and sliding distance of an actual component are calculated using either analytical or numerical methods. The finite element method [1–3] or the elastic foundation method [4,5] is often used for this purpose. Third, wear volume is estimated as a function of service life by combining the wear coefficient with contact pressure and sliding distance. Kim et al. [1] showed this procedure using the tribometer test and finite element analysis and validated the wear profile using the block-on-ring test.

Although this process is commonly applied, the fundamental limitation of wear prediction is that it applies only when the actual contact pressure condition matches the tribometer test (constant) pressure condition. In practice, however, the contact pressure usually varies as a function of time. Furthermore, it often varies over the contact surface. Since the wear coefficient is not an intrinsic material property, it depends on the operating conditions. Calculating wear coefficients at all possible operating conditions requires numerous wear tests and is extremely time consuming. In addition, the variability of wear coefficients is significant even if different parts are made of the same material [6]. Recently, Mukras et al. [7] presented an integrated framework for predicting wear under variable kinematics and kinetics and showed that wear prediction is computationally intensive for varying loads with wear surfaces that change continuously. Thus, it is a preferred approach to measure the wear coefficient directly from the mechanical component in question. Since calculating the wear coefficient requires kinematic information (wear volume and sliding distance) as well as kinetic information (contact force/pressure), it is important to design an in situ measurement apparatus to measure both factors. In this paper, we used an instrumented slider–crank mechanism [8] to measure these factors. Since in situ measurements inherently include uncertainty, we used the Bayesian inference technique [9]

* Corresponding author. Tel.: +1 352 846 0665; fax: +1 352 392 7303.
E-mail address: nkim@ufl.edu (N.H. Kim).

0043-1648/$ – see front matter © 2011 Elsevier B.V. All rights reserved.
doi:10.1016/j.wear.2011.02.010

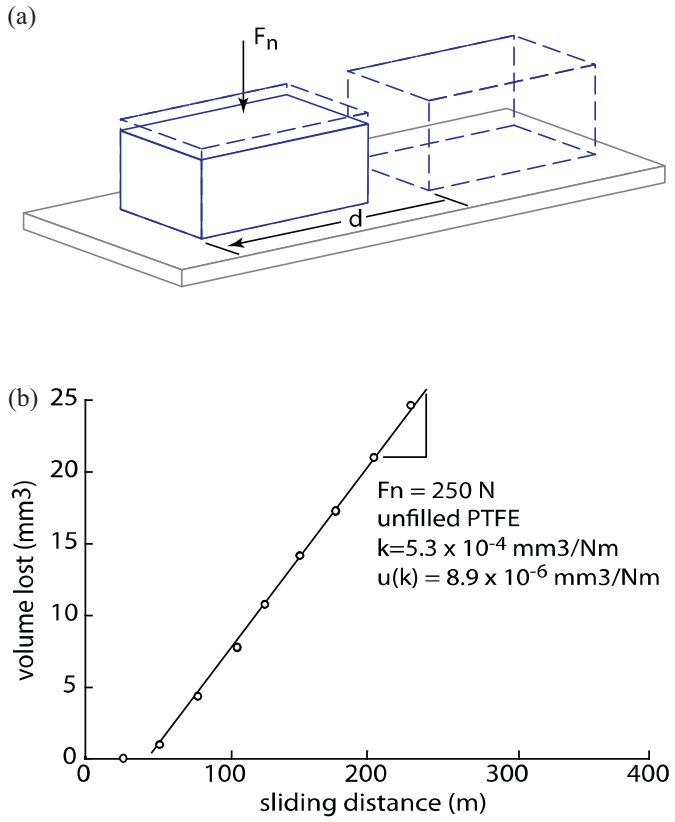

Fig. 1. Tribometer wear test and calculation of wear coefficient. (a) Schematic illustration of tribometer test. (b) An example of wear coefficient data from an unfilled PTFE polymer system [6].

to update the statistical distribution of wear coefficients and predict future wear.

This paper is organized as follows. In Section 2, the simple wear model used in this paper is summarized. Although a linear model is used, the main concept of this paper can be extended to more complex wear models. In Section 3, in situ measurements of joint force and wear volume are presented. Section 4 describes the Bayesian inference technique along with the Markov Chain Monte Carlo (MCMC) method [9]. In Section 5, the wear coefficient is statistically identified and validated. Section 6 includes a discussion of the results and conclusions.

2. Wear model and wear coefficient

Wear is the gradual removal of material; it progresses linearly for many material combinations (mild wear). While various wear phenomena are possible, it is assumed in this paper that all wear cases to be predicted fall within the plastically dominated wear regime, where sliding velocities are small and surface heating is negligible. Archard's wear model [10] is therefore applicable as discussed by Lim and Ashby [11] and Cantizano et al. [12]. Archard's wear model assumes that the volume of material removed is linearly proportional to the product of the slip distance and the normal load. The traditional method for calculating the wear coefficient is shown schematically in Fig. 1. In this model, first published by Holm [13], the worn volume is considered to be proportional to the normal load. The model is expressed mathematically as

$$\frac{V}{s} = K\frac{F}{H}, \tag{1}$$

where V is the worn volume, s is the slip distance, K is the dimensionless wear coefficient, H is the Brinell hardness of the softer material, and F is the applied contact force. Since the wear coefficient is the quantity of interest, Eq. (1) is often written in the following form

$$k = \frac{V}{F \cdot s}. \tag{2}$$

The non-dimensioned wear coefficient K and the hardness are grouped into the dimensioned wear coefficient k. Therefore, the main objective of wear analysis is to identify the wear coefficient for given normal load and slip distance. Since the worn volume is relatively small, it is often measured in the unit of mm^3. Thus, the units of k become $mm^3/N\,m$.

As indicated in Fig. 1, the applied normal force and contact area remain constant through the entire process. If the normal force varies within the slip distance, the definition of wear coefficient in Eq. (2) must be modified as

$$k = \frac{V}{\int_0^s F(s)\ \mathrm{d}s}. \tag{3}$$

In this definition, it is assumed that the wear coefficient is independent of normal force, which is not true in general. However, the wear coefficient k in Eq. (3) can be interpreted as an average wear coefficient for a given load profile.

The wear coefficient is not an intrinsic material property, but instead depends on operating conditions, such as the normal force and slip speed. The value of k for a specific operating condition and given pair of materials may be obtained through experiments [1]. However, experimentation does not often represent the real conditions of a machine, especially when loading conditions vary due to the progress of wear. Thus, a difference may exist between the wear coefficient measured in the tribometer test and that observed from the real machine.

The wear coefficient from the tribometer test is reliable as it is performed under a well-controlled environment, but it may not reflect the real operating conditions. On the other hand, the wear coefficient observed from the real machine reflects real operating conditions, but uncertainty in the field measurements is relatively large as it is not performed under laboratory conditions. The main objective of this paper is to reduce the effect of uncertainty in the field measurements by using a statistical tool to identify the wear coefficient more accurately. The identified wear coefficient can be used to predict the wear volume in the future and, thus, to schedule maintenance intervals.

Table 1
Slider–crank mechanism parameters. Mass moments of inertia are about the center of mass for each body.

Property	Value
Crank mass	0.404 kg
Crank moment of inertia	2.0×10^{-4} kg m^2
Crank length	76.2 mm
Follower mass	0.812 kg
Follower moment of inertia	5.5×10^{-3} kg m^2
Follower length	203.2 mm
Stage mass	8.5 kg
Pin diameter	19.00 mm

3. In situ measurement of joint wear for a slider–crank mechanism

The slider–crank test apparatus used in this study is shown in Fig. 2. The detailed dimensions of the crank and slider are summarized in Table 1. In order to minimize dynamic contributions from the other components in the mechanism, porous carbon air bearings are used for the revolute joint between the follower link and the slide stage, as well as the prismatic joint for the linear slide.

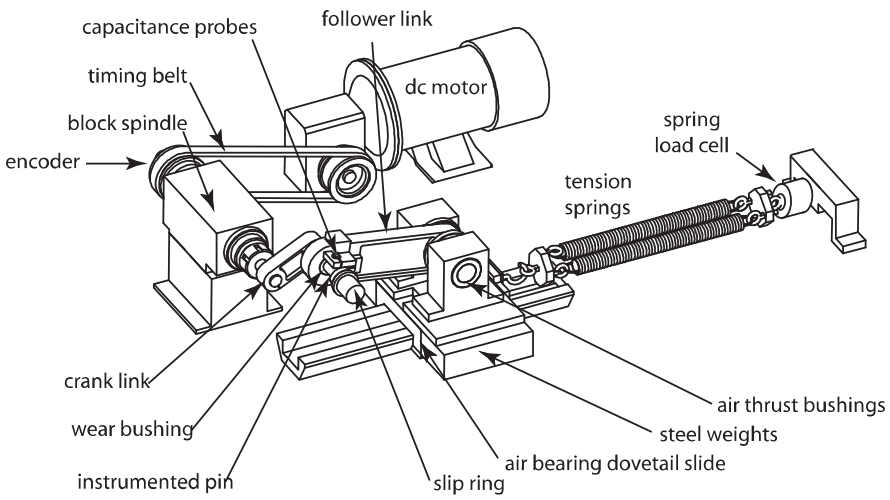

Fig. 2. The layout of slider–crank mechanism used in the experiments.

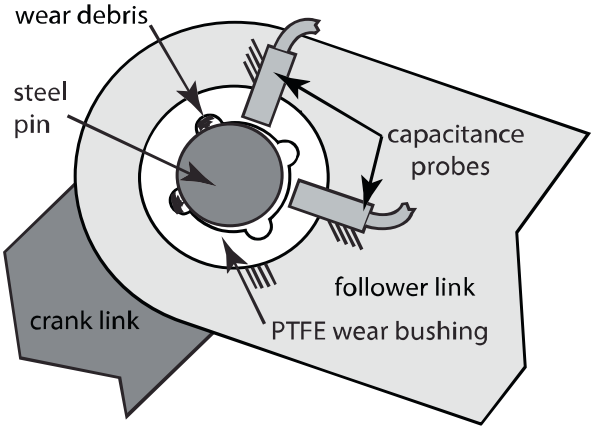

Fig. 3. Capacitance probes measure the location of the pin from fixed locations on the follower link.

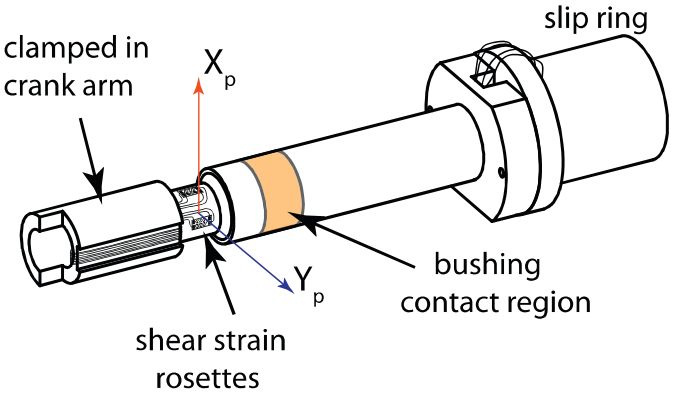

Fig. 4. Instrumented steel pin load cell for measuring joint force.

The revolute joint under study consists of a 19.0 mm diameter instrumented steel pin and a polymer bushing. The pin is clamped in the crank link at one end and rotates, subject to sliding friction, in the bushing clamped in the follower link. The pin is made of hardened steel and is assumed to be hard enough so that no appreciable wear occurs on its surface. The bushing, on the other hand, is made of poly-tetra-fluoro-ethylene (PTFE) which is soft and is subject to considerable wear. To enable the wear debris to escape the contact area and prevent it from affecting the wear progression, grooves are machined into the bushing, as shown in Fig. 3.

The added mass and springs affect the joint force, which can accelerate wear. In practice, mechanisms are usually operated under added masses and additional constraint forces. The wear pattern or process depends on three factors: (1) wear coefficient, (2) joint force and (3) relative motion in the interface. Because different joints may have different joint forces and relative motions, they need to be measured.

Forces transmitted through the joint of interest are measured via a load cell built into a steel pin (Fig. 4). Two full-bridge arrays of strain gages mounted to a necked-down portion of the pin monitor transverse loads while cancelling out bending stresses. The necked portion of the pin, along with a hollow cross section, also serves to localize the strain to the region where the gages are attached. A slip ring mounted to the free end of the pin allows power and signals to be transmitted to and from the strain gages. The load cell is deadweight calibrated and has a full scale capacity of 400 N with a resolution of 2 N.

Simultaneously, two orthogonally mounted capacitance probes monitor the position of the pin relative to bushing (Fig. 3). These probes are clamped to the follower arm and are electrically insulated by polymer bushings. These probes have a range of 1250 μm and a resolution of 40 nm. Additionally, the pin and target are electrically grounded. The angular position of the crank is measured by a hollow shaft incremental encoder attached to the spindle shaft.

Fig. 5 shows the joint force as a function of crank angle at Cycle 1 and Cycle 20,500. The measured joint force agrees well with the multibody dynamic simulation with the coupled evolution wear model (CEWM) [7]. High frequency oscillation is observed when the slider changes its velocity direction. However, there is no significant variation of joint forces between different cycles. Thus, the profile of joint forces is fixed throughout all cycles.

It is well known that uncertainty in applied loading is the most significant factor in prognosis. Without knowing future loadings, the uncertainty in prediction can be so wide that the prediction may not have significant meaning. This issue can be addressed in two ways. First, although the loading condition is variable, if there is enough proof that the future loadings will be similar to the past loadings, then the collected data for past joint forces can be used to predict the future loadings. In this case, the future loadings can be represented using statistical methods. Of course, the uncertainty in predicted life will be increased due to the added uncertainty. Second, wear parameters can be characterized using only the past loading history. This approach is applied here. Note

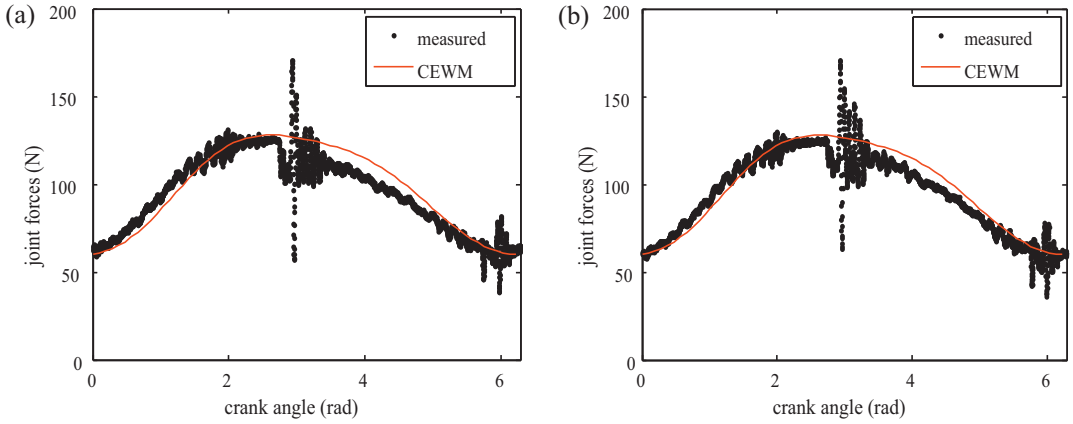

Fig. 5. Joint force predictions and measured data. (a) Cycle 1 and (b) Cycle 20,500.

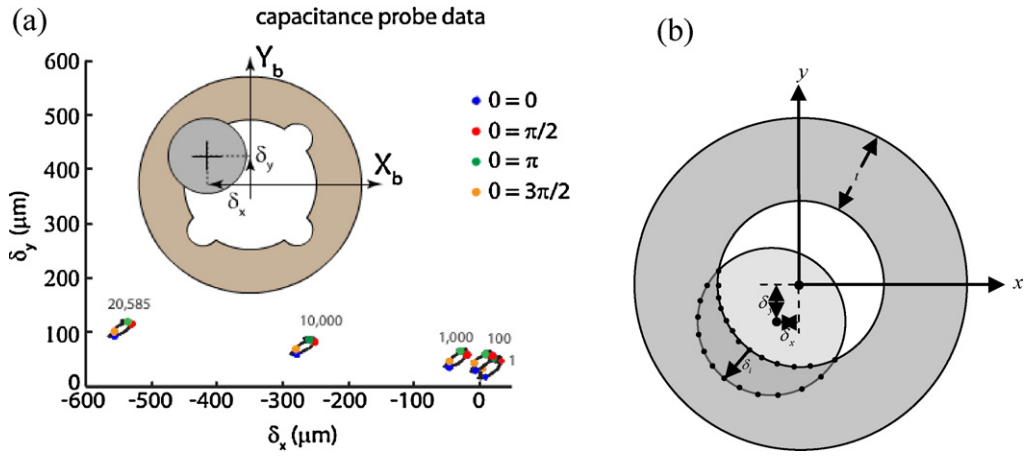

Fig. 6. In situ measurements of pin displacement. (a) Profile of pin center locations. (b) Wear volume from the overlapped area.

Table 2
Wear coefficient calculation using pin locations at 0 radian.

0 radian				
Cycles	Force (N)	Volume (mm^3)	Slip distance (m)	$k \times 10^4$ (mm^3/N m)
1	64.41	1.59	0.06	4134.80
100	62.80	2.57	5.99	68.25
1000	63.17	8.10	59.85	21.44
5000	64.77	24.48	299.24	12.63
10,000	62.65	46.21	598.47	12.32
20,585	59.96	93.90	1232.00	12.71

that this method will also work for a variable load history. In this case, the computation will be more expensive than the current example.

Fig. 6 shows measured displacements of the pin center using the capacitance probe. The wear volume is computed based on the values of δ_x and δ_y. Due to the pre-tensioned springs, the contact points are located at only one side of the bushing. However, the location of pin center varies according to crank angle. This can be explained by the rounded pin surface and different amounts of elastic deformation due to variation in spring forces with crank angle. The measured forces, computed wear volume from the measured displacement, sliding distance and wear coefficient are shown at six cycles for crank angles 0 and π radians in Tables 2 and 3, respectively. Although the wear coefficient converges for both cases, the converged results do not match. This is because the joint force is not constant with angle and the measured wear volume includes uncertainty. In the following section, a statistical approach is introduced to improve the wear coefficient estimate. The idea is to estimate a wear coefficient incorporating uncertainty based on the first five sets of measured data and then predict the wear volume in the sixth cycle using the information. Since the actual data at this cycle are also measured, we can evaluate the accuracy of the method by comparing the measured and predicted results.

4. Bayesian inference for predicting progressive joint wear

4.1. Bayes' theorem

In this study, the Bayesian technique is employed to identify the wear coefficient k using wear volume measurements. The method is based on Bayes' rule as given by Gelman et al. [9], in which the posterior distribution for a given observation can be written as

$$p(\boldsymbol{\theta}|\mathbf{y}) \propto L(\mathbf{y}|\boldsymbol{\theta})p(\boldsymbol{\theta}), \tag{4}$$

Table 3
Wear coefficient calculation using pin locations at π radian.

π radian				
Cycles	Force (N)	Volume (mm^3)	Slip distance (m)	$k \times 10^4$ (mm^3/N m)
1	103.87	7.29	0.06	11731.00
100	106.90	7.64	5.99	119.43
1000	114.04	9.55	59.85	13.99
5000	138.77	23.87	299.24	5.75
10,000	143.50	44.41	598.47	5.17
20,585	147.85	91.56	1232.00	5.03

where $L(\mathbf{y}|\boldsymbol{\theta})$ is the likelihood of observed data $\mathbf{y}$ conditional on the given model parameters $\boldsymbol{\theta}$, $p(\boldsymbol{\theta})$ is the prior distribution of $\boldsymbol{\theta}$, and $p(\boldsymbol{\theta}|\mathbf{y})$ is the posterior distribution of $\boldsymbol{\theta}$ conditional on $\mathbf{y}$. The goal of the Bayesian technique is to improve the knowledge on model parameters $\boldsymbol{\theta}$ using observation $\mathbf{y}$. As more data are provided, the posterior distribution is used as the prior in the next step and the distribution is updated to more confident information. The procedure to obtain the posterior distribution $p(\boldsymbol{\theta}|\mathbf{y})$ consists of proper definition of the probability distribution for the likelihood and prior. In order to satisfy the property of the probability distribution function (PDF), $p(\boldsymbol{\theta}|\mathbf{y})$ needs to be normalized such that the area under the PDF becomes one. In this paper, the wear volume corresponds to the observed data, and the distribution parameters for the wear coefficient correspond to the model parameters.

The likelihood is the probability (or probability density) of obtaining observed data $\mathbf{y}$ for given model parameters $\boldsymbol{\theta}$ and is related to variability in the measurement. The choice of likelihood, probability model, can affect on the analysis results. In this context, Martín and Pérez [14] studied about a generalized lognormal distribution to provide flexible fits to many types of experimental or observational data. Moreover, there are many approaches to select the appropriate distribution type for likelihood. For example, Walker and Gutiérrez-Peña [15] suggested a simple one to select a model when no information on variability of experimental data is available. In this paper, two types of likelihood are assumed for the simplicity: normal and lognormal distributions. In addition to the wear coefficient, the standard deviation of the wear volume is also considered as an unknown model parameter. In the likelihood calculation, the actual wear volume at a given cycle is computed by averaging the values at 0 and π radians (see Tables 2 and 3). Denoting the wear volume measured at the specific cycle as V, the likelihoods of the data for a given wear coefficient and standard deviation can be defined as

$$L(V|k,\ \sigma) \sim N(\mu,\ \sigma) \tag{5}$$

and

$$L(V|k,\ \sigma) \sim LN(\lambda,\ \zeta), \tag{6}$$

where μ and σ are the mean and standard deviation of the wear volume, and λ and ζ are two parameters of the lognormal distribution. Note that $N(\mu,\ \sigma)$ represents a normal distribution, while $LN(\lambda,\ \zeta)$ indicates a lognormal distribution. In Eq. (5), the likelihood is defined with mean and standard deviation. In reality, a single wear volume is measured using in situ capacitance probes, but this measured data has errors. In the likelihood definition, the measured volume is used as a mean value, but the error is unknown. Therefore, the standard deviation of the likelihood is considered unknown and needs to be updated through the Bayesian inference. Therefore, the distribution of standard deviation represents the error in data.

According to Eq. (3), the mean wear volume is expressed as the integral of contact force and slip, multiplied by k. In practice, this integral is computed discretely by dividing the cycle into m equal intervals:

$$\mu = kC\left(\sum_{i=1}^{m} F_i\ \Delta s_i\right). \tag{7}$$

where F_i and Δs_i are the contact force and incremental slip at ith segment, respectively, and C is the number of cycles. Because the force profile is consistent from one cycle to the next, the sum in Eq. (7) is obtained as a constant with the value 5.966 [N m] based on experimental data. In Eq. (6), λ and ζ are given as

$$\lambda = \log\ \mu + \frac{1}{2}\zeta^2 \quad \text{and} \quad \zeta = \sqrt{\log\left(1 + \frac{\sigma^2}{\mu^2}\right)}. \tag{8}$$

Note that the mean is only a function of k since all other terms are given or fixed in Eq. (7). This makes sense given that k and σ are unknown parameters to be estimated conditional on the observed data V.

For the prior distribution of k, specific information from the literature [6] is employed:

$$p(k) \sim N(5.05,\ \ 0.74) \times 10^{-4}. \tag{9}$$

This prior distribution was obtained from tribometer tests under a constant contact pressure to determine k for the bushing with the same material as the current study. In the Bayesian technique, the posterior distribution of k is obtained by multiplying Eq. (5) or (6) with the prior distribution $p(k)$ provided in Eq. (9). Since the Bayesian technique is sensitive to the prior, the case with no prior knowledge (a non-informative prior) is also considered to study the effect of prior information. Additionally, the non-informative prior is considered for the standard deviation σ of likelihood because no knowledge is available. The non-informative prior is equivalent to the uniformly distributed prior that covers entire range. In practice, however, it possible to consider the fist likelihood as a prior distribution.

4.2. Markov Chain Monte Carlo (MCMC) simulation

Even if the expression of posterior distribution is available as a product of likelihood and prior in Eq. (4), the shape of distribution can only be estimated by calculating its values at different points. A primitive way is to compute the values of PDF at a grid of points after identifying the effective range and to calculate the value of the posterior distribution at each grid point. This method, however, has several drawbacks, such as the difficulty in selecting the location, spacing, and scale of the grid points. In addition, it becomes computationally expensive when the number of updating parameters increases. MCMC simulation is a computationally effective alternative which generates a chain of samples to plot the PDF [16]. The Metropolis–Hastings (M–H) algorithm is a common choice for MCMC simulation; it is summarized in Table 4.

In Table 4, $[k^{(0)}, \sigma^{(0)}]$ are the initial values of unknown parameters to be estimated, C is the number of iterations or samples, $U(0, 1)$ is the uniform distribution in the interval of $[0, 1]$, $p(k, \sigma)$ is

Table 4
MCMC simulation process using Metropolis–Hastings algorithm.

1. Initialize $[k^{(0)}, \sigma^{(0)}]$
2. For $i = 0$ to $N - 1$
   - Sample $u \sim U(0, 1)$
   - Sample $[k^*, \sigma^*] \sim q(k^*, \sigma^* | k^{(i)}, \sigma^{(i)})$
   - If $u < \min\left\{1, \frac{p(k^*,\sigma^*)q(k^{(i)},\sigma^{(i)}|k^*,\sigma^*)}{p(k^{(i)},\sigma^{(i)})q(k^*,\sigma^*|k^{(i)},\sigma^{(i)})}\right\}$
     $[k^{(i+1)}, \sigma^{(i+1)}] = [k^*, \sigma^*]$
   - Else
     $[k^{(i+1)}, \sigma^{(i+1)}] = [k^{(i)}, \sigma^{(i)}]$

the posterior distribution, and $q(k, \sigma)$ is an arbitrarily chosen proposal distribution. A uniform distribution is used in this study for the sake of simplicity. Then, $q(k^{(i)}, \sigma^{(i)} | k^*, \sigma^*)$ becomes a uniform distribution centered at $[k^*, \sigma^*]$ with the interval of $\pm\mathbf{w}$, where $\mathbf{w}$ is a vector for setting the sampling interval. The same interval is used for $q(k^*, \sigma^* | k^{(i)}, \sigma^{(i)})$. If the sample $[k^*, \sigma^*]$ is not accepted as an $i+1$th sample, the ith sample becomes the $i+1$th sample; that is, the particular sample is doubly counted.

Since the MCMC method is a sampling-based one, it has to include enough samples so that the statistical characteristics of the distribution can be well captured. There are some methods available to determine the convergence condition, such as El Adlouni et al. [17] and Plummer et al. [18]. In this paper, the convergence condition is determined graphically as the simplest method. It involves discarding the values at the initial stage of iteration, and monitoring the traces and histogram plots for later iterations from which the subjective judgment is made as to the convergence to a stationary chain. As an example of MCMC simulation, we consider a posterior distribution which is given as

$$p(k, \sigma) \propto \left(\frac{1}{\sqrt{2\pi}\sigma}\right)^5 \exp\left[-\frac{1}{2}\sum_{i=1}^{5}\frac{(V_i - kFs)^2}{\sigma^2}\right]. \quad (10)$$

Eq. (10) is the posterior distribution with non-informative prior when the error, ε, between obtained data (in situ wear volume, Vol) and estimated values from wear volume equation (kF_ns) is normally distributed with zero mean and standard deviation, σ. Therefore, the measured wear volume can be represented by

$$Vol = kF_ns + \varepsilon, \quad \varepsilon \sim N(0, \sigma). \quad (11)$$

When n measured data are used, Eq. (10) can be written in a general form as

$$p(k, \sigma) \propto \left(\frac{1}{\sqrt{2\pi}\sigma}\right)^n \exp\left[-\frac{1}{2}\sum_{i=1}^{n}\frac{(V_i - kFs)^2}{\sigma^2}\right]. \quad (12)$$

If n is one, the equation is exactly same with normal distribution. Eq. (10) is the case that n is five, which is obtained by multiplying Eq. (12) with $n = 1$ five times. Fig. 7 and Table 5 show the sampling result of $[k, \sigma]$ for Eq. (10).

Fig. 7(a) represents traces of 10,000 sample iterations. As mentioned previously, the initial stages are discarded because they are not converged; the discarding value can be selected as an arbitrary value, in this case we select 4000 as the discarding value. Fig. 7(b) gives the estimated PDF with 6000 samples from 4001 iterations, while Fig. 7(c) shows the analytical PDF from Eq. (10). It can be seen that the MCMC sampling result follows the analytical distribution quite well. Table 5 shows that the first statistical moments have less than 1% error.

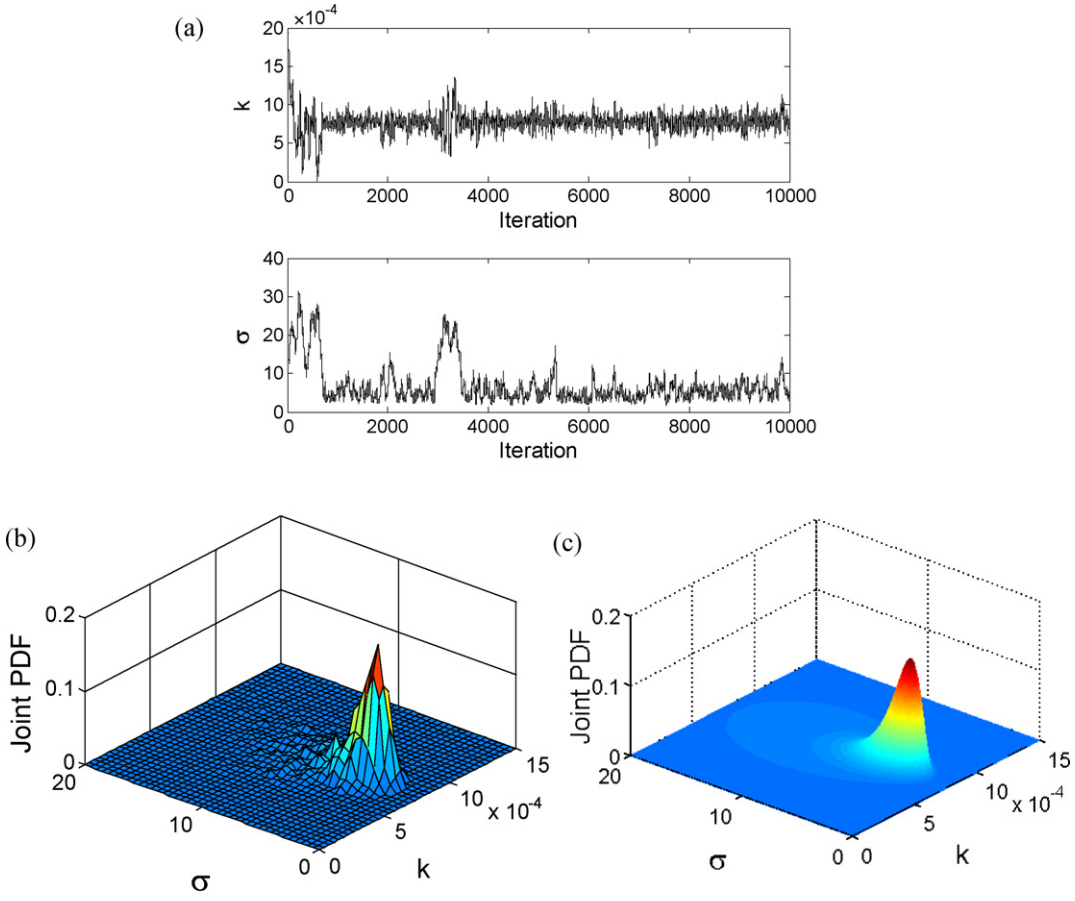

Fig. 7. Joint posterior PDF. (a) Trace of iteration. (b) Using MCMC. (c) Exact solution.

Table 5
Statistical moments.

	μ_k	μ_σ	σ_k	σ_σ	cov(k, σ)
MCMC	7.82×10^{-4}	5.61	0.93×10^{-4}	2.59	0
Exact sol.	7.76×10^{-4}	5.63	0.92×10^{-4}	2.51	0
Error (%)	0.79	0.47	1.09	3.13	0

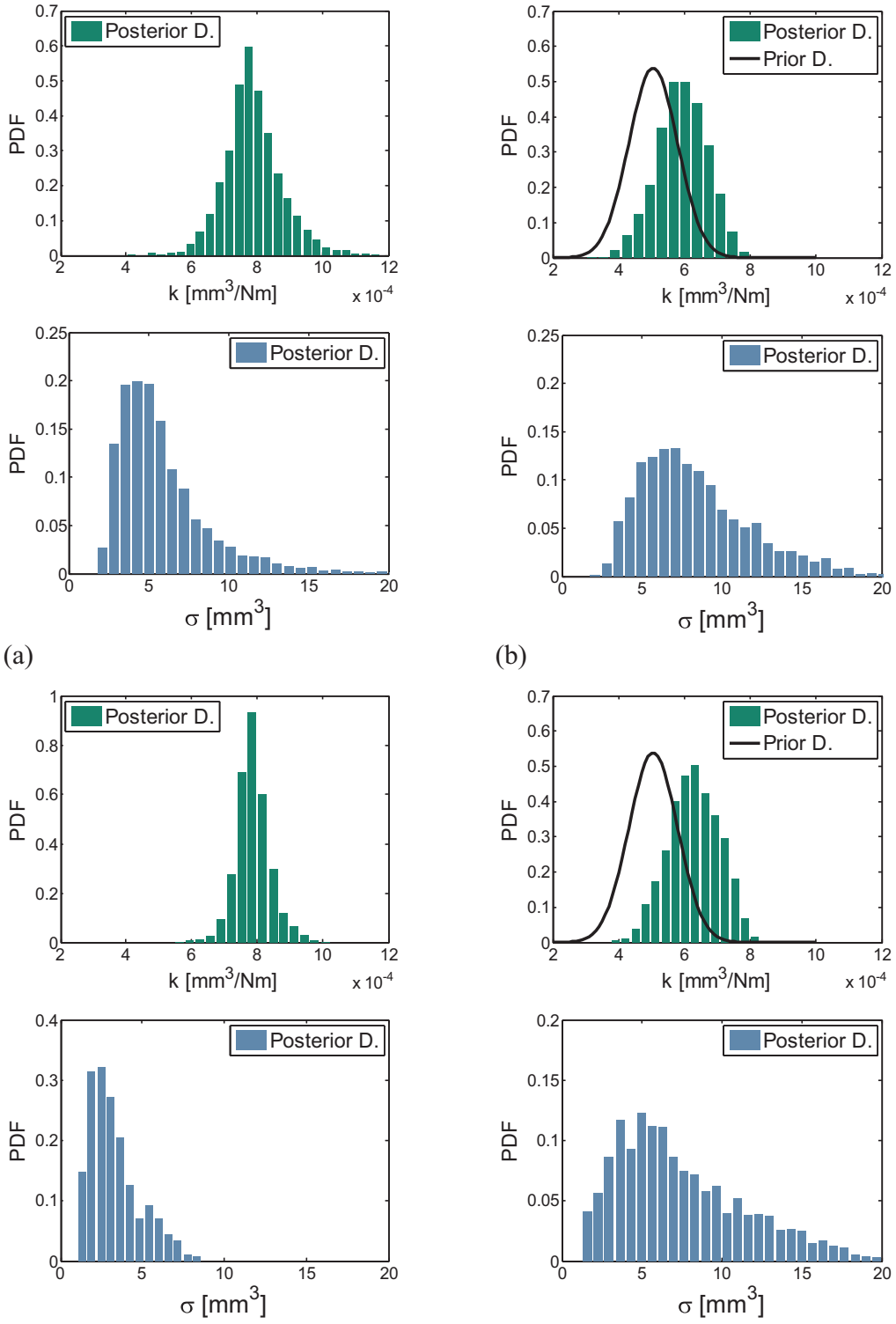

Fig. 8. Posterior distribution when using the first five data sets. (a) Normal likelihood with non-informative prior. (b) Normal likelihood with normal prior. (c) Lognormal likelihood with non-informative prior. (d) Lognormal likelihood with normal prior.

Table 6
Mean and standard deviation of k (10^{-4} mm^3/N m).

Likelihood	Prior	Data set number	3	4	5	6
Normal	Non-inform.	Mean	17.49	8.28	7.89	7.57
		Std.	10.02	2.32	0.90	0.40
	Prior	Mean	5.11	5.42	5.93	6.89
		Std.	0.73	0.73	0.76	0.57
Lognormal	Non-inform.	Mean	20.81	8.89	7.88	7.64
		Std.	5.82	1.17	0.51	0.25
	Prior	Mean	5.46	5.67	6.29	7.41
		Std.	0.72	0.75	0.77	0.25

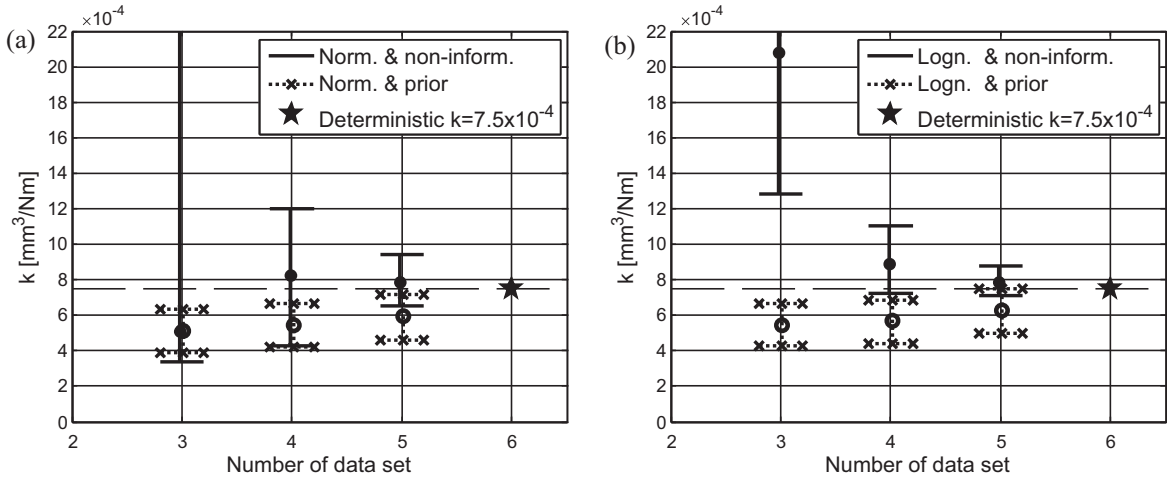

Fig. 9. Confidence intervals of the wear coefficient in terms of the data set number. (a) Likelihood: normal distribution. (b) Likelihood: lognormal distribution.

Once the samples are obtained from the posterior distribution of $[k, \sigma]$, the samples of wear volume can be obtained by using Eq. (3) or Eq. (7). In Eq. (7), μ represents the wear volume which is obtained as a distribution due to the uncertainty of unknown parameter, k, and the 90% interval is defined as a confidence interval (CI). The level of prediction interval (PI) can also be calculated by adding the measurement error σ to the wear volume in Eq. (7).

5. Identification of wear coefficient and prediction of wear volume

5.1. Posterior distribution of wear coefficient

The posterior distributions of k and σ are obtained as the results of five times updating using the MCMC technique with the first five sets of data in Tables 2 and 3. The last data set is remotely located and is used for the prediction validation. In the MCMC process, the number of iterations is fixed at 10,000. The resulting PDFs are given in Fig. 8. Both normal and lognormal distributions are considered for the likelihood, and both non-informative and normal distributions are considered for the prior. In the case of a non-informative prior, the PDF shape in Fig. 8(c) with the lognormal likelihood is narrower than that of Fig. 8(a) with the normal likelihood. As shown in the fifth set of Table 6, the standard deviation from the lognormal likelihood (0.51×10^{-4} mm^3/N m) is 43% less than that of normal likelihood (0.9×10^{-4} mm^3/N m), whereas the mean values are nearly equal; i.e., 7.89 and 7.88, respectively. These results show that the lognormal likelihood exhibits increased accuracy over the normal likelihood. The reason that the former is better than the latter may be attributed to the non-negative nature of the lognormal distribution, which is the case of the wear coefficient.

By comparing the results for the two priors, i.e., Fig. 8(a) vs. Fig. 8(b) and Fig. 8(c) vs. Fig. 8(d), it is seen that the use of a normal prior leads to underestimation of the mean for k. It is noted that the actual k values at the last data set are found to vary between 5.03×10^{-4} and 12.71×10^{-4} (see Tables 2 and 3), of which the average is 8.5×10^{-4}. The reason that the results with a prior are worse than the non-informative results may be attributed to the inaccurate prior distribution; as mentioned previously, the tribometer wear tests were performed under the uniform pressure condition, while the contact pressure in the bushing is not constant. In addition, the wear coefficient is not an intrinsic material property, but depends on contact pressure and contact area. It is also observed that the posterior distributions of k in Fig. 8(a) and (c) are close to Laplacian distribution with heavy tails. Although the case with lognormal likelihood has narrower distribution, the type of distribution is very close. On the other hand, the posterior distributions with the normal prior in Fig. 8(b) and (d) show quite different distribution type. Therefore, it can be concluded that the prior contributes significantly to the posterior distribution. This is partly related to the fact that the prior information is not consistent with observed data.

In order to investigate the effects of the prior in more detail, the posterior distributions of k are obtained after updating at each data set. Values of the mean and standard deviation are given in Table 6, and 5%/95% percentiles as well as maximum likelihood values are plotted in Fig. 9. In Fig. 9, the star maker denotes the mean value of the distribution after the last update; i.e., using the sixth data set. This is used as a target value for correct prediction of the earlier stage.

In Fig. 9(a) and (b), the confidence intervals with the normally distributed prior are located much lower than the ones without a prior (non-informative) and do not include the target value. What is remarkable from this observation is that, although the use of prior knowledge is usually recommended to accommodate more confidence and faster convergence, it should be used with caution. In this study, the wear coefficient is not an intrinsic material property but can vary with operating conditions. This turned out to be the

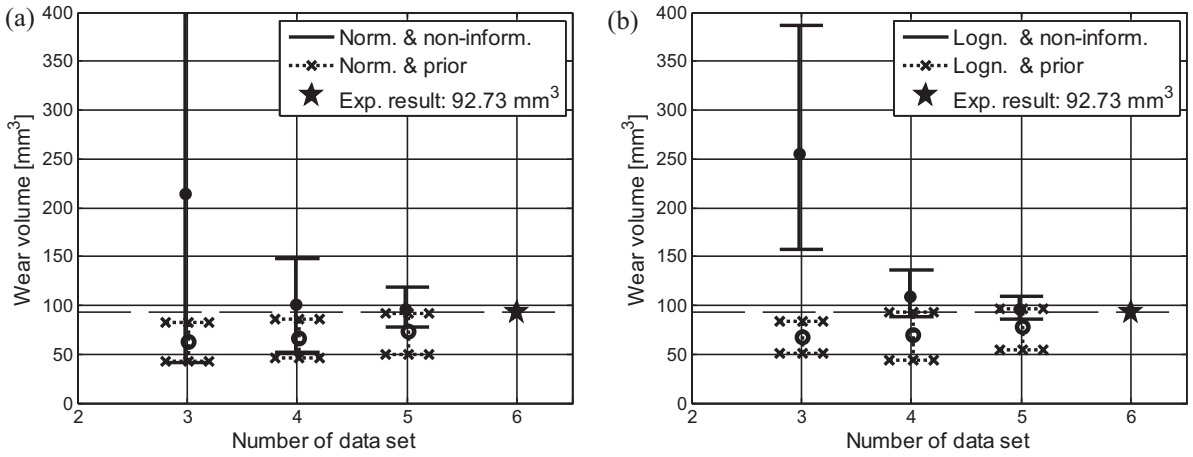

Fig. 10. Prediction intervals of the wear volume at 20,585 cycles in terms of the data set number. (a) Likelihood: normal distribution. (b) Likelihood: lognormal distribution.

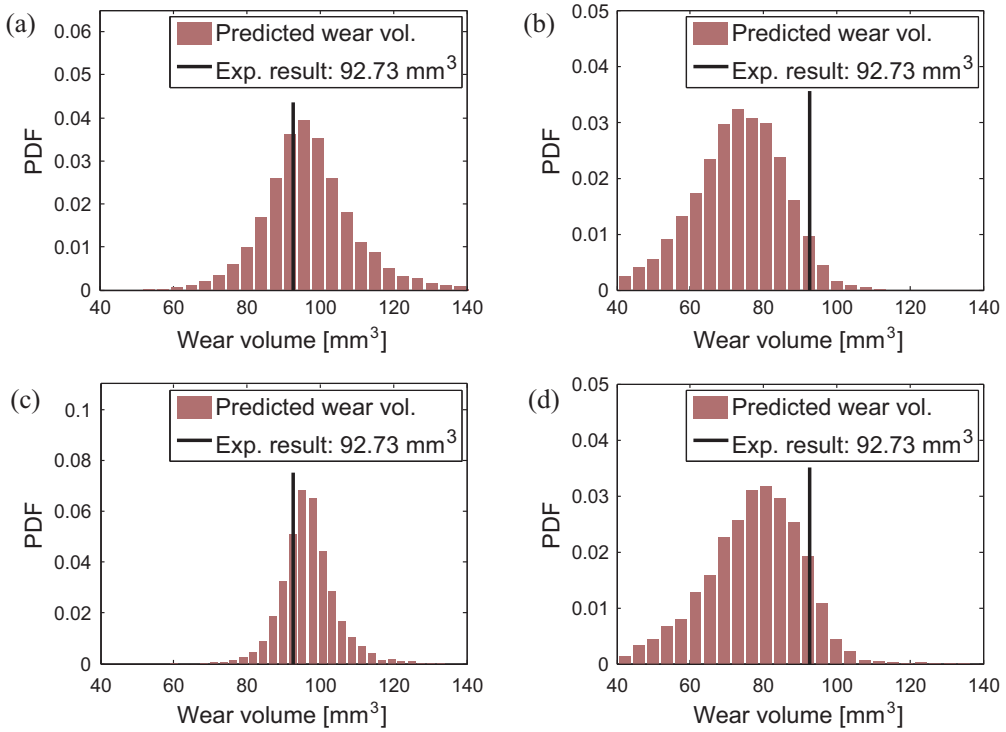

Fig. 11. Predicted distributions of wear volume at cycle = 20,565. (a) Likelihood: *N* and non-inform. (b) Likelihood: *N* and prior. (c) Likelihood: *LN* and non-inform. (d) Likelihood: *LN* and prior.

cause of incorrect prediction, and should be avoided. It should be noted, however, that this is not always the case. Unlike the present case, if only limited data are available, the user may have to depend more on prior knowledge than the likelihood of the data.

5.2. Posterior prediction of wear volume

Once the posterior distribution of k and σ are obtained, the information can be used to predict the wear volume at the next stage. For that purpose, the wear volume for the sixth data set (20,585 cycles) is predicted using the posterior distribution for the wear coefficient from previous data sets. Due to the uncertainty in k and σ, the predicted wear volume is a distribution. Fig. 10 shows 5%/95% percentiles and maximum likelihood values of the wear volume distribution. In the figure, the actual value of wear volume measured at the sixth data set (92.73 mm^3) is used as a target value. As noted previously, the use of selected prior does not predict the wear volume well. Even the upper confidence limit is below the target value, which can cause unexpected failure if the value is carelessly used in the design decision.

Comparing the results of normal and lognormal likelihood, the size of the interval is quite large at the third stage of data in the case of the normal likelihood. However, the size of the interval is quickly reduced as the number of data set increases. Overall, the size of the interval of the lognormal likelihood is smaller than that of the normal likelihood.

In Fig. 11, the predicted distributions of the wear volume at the sixth stage using the posterior distributions from the fifth stage are given with different combinations of likelihoods and priors; the line indicates the measured value. It can be seen that the result with the non-informative prior is better than that with the normally distributed prior. Due to the underestimation of the wear coefficient

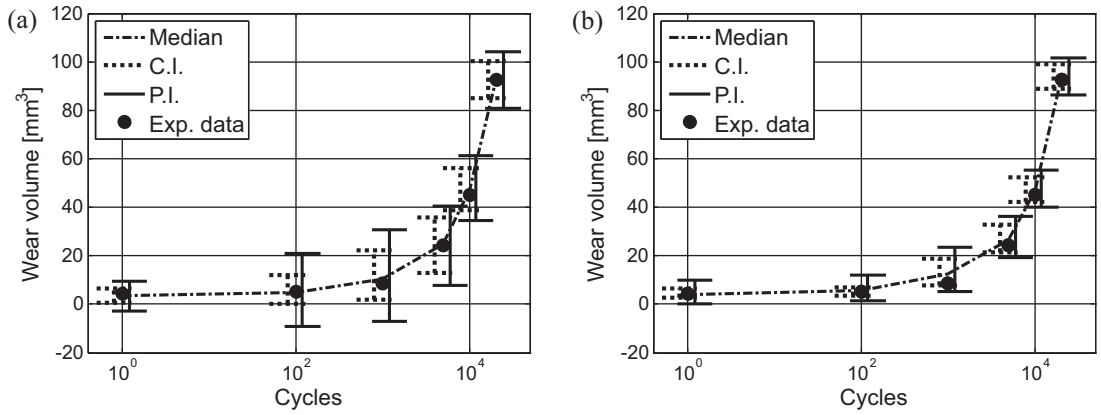

Fig. 12. Confidence and prediction intervals of wear volume. (a) Likelihood: normal distribution. (b) Likelihood: lognormal distribution.

Table 7
CI and PI of wear volume.

Data set number			1	2	3	4	5	6
Measured wear V			4.44	5.105	8.825	24.175	45.31	92.73
CI	*N*	95%	6.61	12.13	22.14	35.75	56.25	100.38
		5%	0.75	0.35	2.03	12.78	38.87	85.09
		Inter	5.86	11.77	20.11	22.97	17.38	15.28
	LN	95%	6.61	7.06	18.73	32.88	52.27	99.04
		5%	2.50	3.60	7.66	21.52	42.31	88.78
		Inter	4.11	3.46	11.07	11.36	9.96	10.26
PI	*N*	95%	9.19	20.32	30.96	40.34	60.64	104.04
		5%	−2.84	−9.18	−7.01	7.56	33.78	81.22
		Inter	12.03	29.50	37.97	32.78	26.87	22.82
	LN	95%	9.90	12.22	23.72	36.06	55.18	101.86
		5%	0.24	1.23	5.18	19.36	39.87	86.70
		Inter	9.66	10.99	18.53	16.70	15.30	15.15

in the normally distributed prior, the predicted wear volumes with the prior are less than the actual one.

In Fig. 12, the confidence interval (CI) and prediction interval (PI) of the wear volumes at all stages are given using the posterior distribution at each stage along with the measured data (denoted by dots). In both cases of likelihoods, the CI and PI have a tendency to gradually decrease from 1000 cycles as the cycles increase. The results at the first and second stages, which are 1 cycle and 100 cycles, respectively, exhibit smaller intervals than other high cycles even if they are results with small data. The reason is that the variances of the parameters are large, but the wear volume itself is very small at low cycle compared to higher cycles. Although these early stages are not of interest in terms of prognosis, the estimation results are fairly exact. In Table 7, the numerical values of CI and PI are provided. The CIs and PIs of the lognormal case are smaller than that of the normal case, which demonstrates improved accuracy.

6. Discussions and conclusions

In this paper the Bayesian inference technique is used to estimate the probability distribution of wear coefficients from in situ measurements. The first five sets of data up to 10,000 cycles are used to reduce uncertainty in wear coefficient and the last set of data at 20,585 cycles is used for the prediction validation. The numerical results show that the posterior distribution with a non-informative prior is more accurate than that with the prior distribution from the literature. This result is obtained because the converged posterior distribution is quite different from the prior distribution. In order to predict the wear coefficient of a mechanical component, it has been suggested that the wear volume, slip distance and applied load must be measured simultaneously.

Acknowledgments

This work was supported by the National Research Foundation of Korea (NRF) grant funded by the Korea Government (MEST) (No. 2009-0081438), Deere and Company, and National Science Foundation (CMMI-0600375).

References

[1] N.H. Kim, D. Won, D. Buris, B. Holtkamp, G.R. Gessel, P. Swanson, W.G. Sawyer, Finite element analysis and validation of metal/metal wear in oscillatory contacts, Wear 258 (11–12) (2005) 1787–1793.
[2] P. Podra, S. Andersson, Finite element analysis wear simulation of a conical spinning contact considering surface topography, Wear 224 (1999) 13–21.
[3] P. Podra, S. Andersson, Simulating sliding wear with finite element method, Tribology International 32 (1999) 71–81.
[4] Y. Bei, B.J. Fregly, W.G. Sawyer, S.A. Banks, N.H. Kim, The relationship between contact pressure, insert thickness, and mild wear in total knee replacements, Computer Modeling in Engineering and Science 6 (2) (2004) 145–152.
[5] S. Mukras, N.H. Kim, N.A. Mauntler, T. Schmitz, W.G. Sawyer, Comparison between elastic foundation and contact force models in wear analysis of planar multibody system, Journal of Tribology 132 (3) (2010) 031604-1–031604-11, doi:10.1115/1.4001786.
[6] T.L. Schmitz, W.G. Sawyer, J.E. Action, J.C. Ziegert, Wear rate uncertainty analysis, Journal of Tribology 126 (2004) 802–808.
[7] S. Mukras, N.H. Kim, N.A. Mauntler, T. Schmitz, W.G. Sawyer, Analysis of planar multibody systems with revolute joint wear, Wear 268 (5–6) (2010) 643–652.
[8] N. Mauntler, N.H. Kim, W.G. Sawyer, T.L. Schmitz, An instrumented crank–slider mechanism for validation of a combined finite element and wear model, in: Proceedings of 22nd Annual Meeting of American Society of Precision Engineering, Dallas, Texas, October 14–19, 2007.
[9] A. Gelman, J.B. Carlim, H.S. Stern, D.B. Rubin, Bayesian Data Analysis, second ed., Chapman & Hall/CRC, New York, 2004.
[10] J.F. Archard, Contact and rubbing of flat surfaces, Journal of Applied Physics 24 (1953) 981–988.
[11] S.C. Lim, M.F. Ashby, Wear-mechanism maps, Acta Metallurgica 35 (1987) 1–24.
[12] A. Cantizano, A. Carnicero, G. Zavarise, Numerical simulation of wear-mechanism maps, Computational Materials Science 25 (2002) 54–60.

[13] R. Holm, Electric Contacts, Almqvist & Wiksells Boktryckeri, Uppsala, 1946.
[14] J. Martín, C. Pérez, Bayesian analysis of a generalized lognormal distribution, Computational Statistics and Data Analysis 53 (2009) 1377–1387.
[15] S.G. Walker, E. Gutiérrez-Peña, Robustifying Bayesian procedures, in: J.M. Bernardo, J.O. Berger, A.P. Darwin, A.F.M. Smith (Eds.), Bayesian Statistics, vol. 6, Oxford University Press, Oxford, 1999, pp. 685–710.
[16] C. Andrieu, N. de Freitas, A. Doucet, M. Jordan, An introduction to MCMC for machine learning, Machine Learning 50 (2003) 5–43.
[17] S. El Adlouni, A.C. Favre, B. Bobe, Comparison of methodologies to assess the convergence of Markov Chain Monte Carlo methods, Computational Statistics & Data Analysis 50 (10) (2006) 2685–2701.
[18] M. Plummer, N. Best, K. Cowles, K. Vines, CODA: convergence diagnosis and output analysis for MCMC, R News 6 (1) (2006) 7–11.